Fuchs, S., Förster, H.-J., Braune, K., Förster, A. (2018): Calculation of Thermal Conductivity of Low-Porous, Isotropic Plutonic Rocks of the Crust at Ambient Conditions From Modal Mineralogy and Porosity: A Viable Alternative for Direct Measurement? - *Journal of Geophysical Research*, *123*, 10, pp. 8602—8614.

DOI: http://doi.org/10.1029/2018JB016287

Journal of Geophysical Research: Solid Earth

RESEARCH ARTICLE
10.1029/2018JB016287

Special Section:
Physical Properties of Rocks, Friction and Fracturing: The Walsh Volume

Key Points:
- Modal mineralogy permits matrix thermal conductivity (λ) calculation with 2σ-uncertainty of <15% using the harmonic-mean model
- Uncertainty is reduced to <10% if rock porosity is implemented in the calculation procedure
- Method is particularly valuable for inferring λ of drill cuttings and enclaves, promoting heat-flow calculation and geotherm computation

Correspondence to:
S. Fuchs,
fuchs@gfz-potsdam.de

Citation:
Fuchs, S., Förster, H. -J., Braune, K., & Förster, A. (2018). Calculation of thermal conductivity of low-porous, isotropic plutonic rocks of the crust at ambient conditions from modal mineralogy and porosity: A viable alternative for direct measurement? *Journal of Geophysical Research: Solid Earth*, *123*, 8602–8614. https://doi.org/10.1029/2018JB016287

Received 28 JUN 2018
Accepted 19 SEP 2018
Accepted article online 24 SEP 2018
Published online 29 OCT 2018

Calculation of Thermal Conductivity of Low-Porous, Isotropic Plutonic Rocks of the Crust at Ambient Conditions From Modal Mineralogy and Porosity: A Viable Alternative for Direct Measurement?

S. Fuchs[1], H. -J. Förster[1], K. Braune[2], and A. Förster[1]

[1]Helmholtz Centre Potsdam, German Research Centre for Geosciences GFZ, Potsdam, Germany, [2]Institute of Earth and Environmental Science, University of Potsdam, Potsdam, Germany

Abstract Thermal conductivity (λ) is an essential physical property of minerals and rocks and fundamental in constraining the thermal field of the lithosphere. In case that adequate samples to measure λ are not available, it could be indirectly inferred from calculation. One of the most widely applied indirect methods for rocks involve modal mineralogy and porosity as parameters that are incorporated into mathematical mean or mixing models. Robust inferences from these approaches for crystalline rocks were impeded by a small number of studied samples or restriction to certain rock types. We employ this method and examine its applicability to low-porosity plutonic rocks by calculating bulk thermal conductivity λ_b for 45 samples covering the entire range from gabbro/diorite to granite. We show that the use of the harmonic-mean model for both rock matrix and porosity provided a good match between $\lambda_{b.meas}$ and $\lambda_{b.calc}$ of <10% deviation (2σ), with relative and absolute errors amounting to 1.4 ± 9.7% and 4.4 ± 4.9%, respectively. The results of our study constitute a big step forward to a robust conclusion on the overall applicability of the harmonic-mean model for inferring λ_b of isotropic, low-porosity, mafic to silicic plutonic and metamorphic rocks with an acceptable magnitude of error. Drill cuttings and enclaves form particularly interesting objects for application of this method, as they are poorly suited for direct λ measurement. Well-derived λ values for those rocks would permit to calculate heat flow and to model more profoundly the thermal state of the deeper lithosphere.

1. Introduction

Thermal conductivity (λ) is, alongside with thermal diffusivity, thermal effusivity, specific heat, and volumetric heat capacity, a fundamental physical property of minerals and rocks. It is essential for the calculation of heat flow, which represents an indispensable parameter in modeling the thermal field and, thus, constraining rheological and seismic properties of a region. Understanding the thermal structure of any geologic setting requires accurate knowledge of λ of all involved geological units. Precise λ data are not only inevitable for quantifying the thermal evolution of crystalline areas and sedimentary basins, but with increasing importance also in mining, geotechnical, underground, and civil engineering (Popov et al., 2016). Proper designing of nuclear-waste repository systems, the exploration for geothermal energy, or the safe underground storage of fluid and gaseous media all require accurate information of rock thermal properties.

Thermal conductivity can be inferred from various direct and indirect methods. The three most commonly applied direct methods at ambient conditions are the optical-scanning, the divided-bar, and the line-source method (Popov et al., 2016, and references therein). Indirect approaches are used, if direct measurements of λ cannot be performed. Those approaches infer λ from (I) data on mineralogical composition, porosity, and composition of saturation fluids deploying numerical mixing models or from (II) correlations of λ with other physical properties. Studies pertaining to group-I have addressed low-porous granitic and metamorphic rocks (Chopra et al., 2018; Drury & Jessop, 1983; Pribnow & Umsonst, 1993; Ray et al., 2015; Zhao et al., 2016). Applications to sedimentary rocks have focused on models to determine bulk (or effective) thermal conductivity (λ_b) from matrix conductivity (λ_m) and varying porosity (e.g., Albert et al., 2017; Fuchs et al., 2013; Merkle et al., 1976). Group-II methods mostly deployed data from sedimentary rocks measured in boreholes (e.g., Anand et al., 1973; Evans, 1977; Fuchs et al., 2015; Goss et al., 1975;

Table 1
Rock Type and Location of Samples

#	Sample #	Rock type	Location
1	Z5b	granite	Fichtelgebirge, DE
2	L13	granite	Leuchtenberg, Oberpfalz, DE
3	M5B	granite	Mitterteich, Oberpfalz, DEU
4	Hzb1	granite	Hauzenberg, Passauer Wald, DE
5	ARN	granite	Arnbruck, Bayrischer Wald, DE
6	IMS-1	granite	Ilimaussaq, Grreenland, DK
7	Lu-1	granite	Lusen, Bayrischer Wald, DE
8	L2	granite	Leuchtenberg, Oberpfalz, DE
9	EHR-2	granite	Eberhartsrent, Bayrischer Wald, DE
10	NE4	granite	Neunburg, Oberpfalz, DE
11	TI-2	granite	Fürstenstein, Bayrischer Wald, DE
12	PAG	granodiorite	Patersdorf, Bayrischer Wald, DE
13	428	granodiorite	Görlitz, Ostlausitzer Massiv, DE
14	SD1	granodiorite	Schärding, Mühlviertel, AU
15	TM2	granodiorite	Turga massif, Transbaikalia, RU
16	PADR1	granodiorite	Patersdorf, Bayrischer Wald, DE
17	603	granodiorite	Kurakusik, Tian Shan, KG
18	DP68	granodiorite	Hubayra, Aquaba-Araba complex, JO
19	599	monzonite	Izbairamski complex, Tian Shan, KG
20	Cs-2	syenite	Jiazishan, Shidao Complex, CN
21	Cs-3	syenite	Jiazishan, Shidao Complex, CN
22	1317	quartz monzodiorite	Meissner massif, Elbe Zone, DE
23	DP49	quartz monzodiorite	Um Rachel, Aquaba-Araba complex, JO
24	1325	quartz monzodiorite	Meissen massif, Elbe Zone, DE
25	WSN1	granodiorite	Weschnitz pluton, Odenwald, DE
26	594	tonalite	Malchen, Odenwald, DE
27	Fü1b	monzodiorite	Fürstenstein, Passauer Wald, DE
28	GM1684	monzonite	Isortoq, Greenland, DK
29	DP71	quartz anorthosite	Marsod, Aquaba-Araba complex, JO
30	R4B	diorite	Reuth, Oberpfalz, DE
31	DP65	quartz monzodiorite	Taur, Aquaba-Araba complex, JO
32	1327	monzodiorite	Meissen massif, Elbe Zone, DE
33	TMZ1	tonalite	Tamazeght complex, MA
34	598	quartz monzodiorite	Izbairamski complex, Tian Shan, KG
35	KH49	nepheline syenite	Ilimaussaq, Greenland, DK
36	597	monzodiorite	Izbairamski complex, Tian Shan, KG
37	Cs-1	alkali gabbro	Shidao Complex, CN
38	Rhu4	gabbro	Isle of Rum, Scotland, UK
39	EDB1	alkali gabbro	Edinburgh, Scotland, UK
40	FTG1	quartz monzodiorite	Ochsenkopf, Fichtelgebirge, DE
41	GM1803	gabbro	Isortoq, Greenland, DK
42	Rhu2	gabbro	Isle of Rum, Scotland, UK
43	1319	gabbro	Meissen massif, Elbe Zone, DE
44	SRH1	gabbro	Schriesheim, Odenwald, DE
45	FRS1	gabbro	Frankenstein, Odenwald, DE

Note. DE = Germany; DK = Denmark; AU = Austria; RU = Russia; KG = Kirkisistan; JO = Jordan; CN = China; MA = Marocco; UK = United Kingdom.

Hartmann et al., 2005). A comprehensive list of references and a detailed discussion on the pros and cons of well-log derived λ estimation are provided by Fuchs and Förster (2014). In contrast to work in sedimentary settings, adequate studies in hard rocks are scarce (Gegenhuber & Kienler, 2017; Pribnow et al., 1993; Williams & Anderson, 1990).

Previous approaches to infer λ from quantitative data on modal mineralogy of low-porous hard rocks by applying mixing models (group I) were conflicted with one or more of the following limitations: (a) the study included only few types of rock, that is, granites, high-grade metamorphic rocks, etc.; (b) the samples represented single batholiths or geological provinces, thus were regionally limited; (c) the study involved only a limited number of samples; and (d) the study evaluated only a few of the commonly used mixing models.

Although all yet practiced indirect approaches are rated as not matching the accuracy and precision of carefully performed laboratory measurements (Popov et al., 2016), they constitute the only option to get reasonable λ values in case that samples appropriate for direct measurement are not at disposal. Samples unsuited or less suited for measurement include, for instance, tiny drill cuttings, mechanically weakened rocks, or small-sized enclaves and xenoliths.

This paper reports the result of seeking out the mixing model(s) providing the best match between measured ($\lambda_{b.meas}$) and calculated bulk thermal conductivity ($\lambda_{b.calc}$) for low-porous, igneous crustal rocks. All samples were confirmed being isotropic, that is, display identical (within limit of measurement error) of λ in all directions. The study encompassed 45 samples representing various geological provinces in eight countries (Table 1). In contrast to previous studies, our suite of samples covers the entire range from mafic (gabbro/diorite) to silicic rocks (granite), straddling the range 36–76 wt.% SiO_2 (corresponding quartz range: 0–45 vol.%), and includes both such of alkaline, peralkaline, metaluminous, and peraluminous affinity. Assessment of the quality of fit involved all frequently applied mixing models that consider quantitative data on modal mineralogy. Our evaluation clearly demonstrates that λ_b of low-porous igneous rocks, irrespective of being mafic or felsic, could be indirectly calculated from their mineral content with an acceptable error by employing the harmonic mean model.

2. Methodology and Samples

We explored the usability of the following mean models (abbreviations in parentheses) for indirect λ_b calculation, where X_i is the volume fraction of the *i*th phase relative to the total volume ($\sum X_i = 1$). The physical and/or empirical backgrounds of these models have been comprehensively described by Abdulagatova et al. (2009) and Clauser (2009) in connection with computation of λ.

Arithmetic mean (AM; Reuss, 1929; Voigt, 1928):

$$\lambda_{AM} = \Sigma_{i=1}^{n} X_i \lambda_i \tag{1}$$

Harmonic mean (HM; Reuss, 1929; Voigt, 1928):

$$\lambda_{HM} = 1/\Sigma_{i=1}^{n} \frac{X_i}{\lambda_i} \tag{2}$$

Voigt-Reuss-Hill average (VRH; Hill, 1952):

$$\lambda_{VRH} = \frac{1}{2}(\lambda_{AM} + \lambda_{HM}) \tag{3}$$

Geometric mean (GM; Lichtenecker, 1924):

$$\lambda_{GM} = \Pi_{i=1}^{n} \lambda^{X_i} \tag{4}$$

Square-Root-Mean (SQR; Roy et al., 1981):

$$\lambda_{SQR} = \left(X_i \sqrt{\lambda_i}\right)^2 \tag{5}$$

Effective Medium Mean (Eff, Bruggeman, 1935)

$$\lambda_{Eff}^{-1} = \Sigma_{i=1}^{n} \frac{3X_i}{2\lambda_{VRH} + \lambda_i} \tag{6}$$

Hashin and Shtrikman mean (HS; Hashin & Shtrikman, 1962)

$$\lambda_{HS} = \frac{1}{2}(\lambda_{HSU} + \lambda_{HSL}) \tag{7}$$

with the upper boundary:

$$\lambda_{HSU} = \lambda_{max} + \frac{A_{max}}{1 - \alpha_{max} A_{max}} \tag{8}$$

$$A_{max} = \Sigma_{i=1;\lambda_i \neq \lambda_{max}}^{n} \frac{X_i}{\alpha_{max} + 1/(\lambda_i - \lambda_{max})}; \tag{9}$$

$$\alpha_{max} = \frac{1}{3\lambda_{max}}; \tag{10}$$

and with the lower boundary

$$\lambda_{HSL} = \lambda_{min} + \frac{A_{min}}{1 - \alpha_{min} A_{min}} \tag{11}$$

$$A_{min} = \Sigma_{i=1;\lambda_i \neq \lambda_{min}}^{n} \frac{X_i}{\alpha_{min} + 1/(\lambda_i - \lambda_{min})}; \tag{12}$$

$$\alpha_{min} = \frac{1}{3\lambda_{min}}; \tag{13}$$

Herein, $\lambda_{min} =$ min $(\lambda_1, \ldots, \lambda_n)$ and $\lambda_{max} =$ max $(\lambda_1, \ldots, \lambda_n)$.

Table 2
Whole-Rock Geochemistry (wt.%)

#	Sample #	SiO_2	TiO_2	Al_2O_3	Fe_2O_3	MnO	MgO	CaO	Na_2O	K_2O	P_2O_5	H_2O^+	CO_2	Total
1	Z5b	76.10	0.12	12.60	1.82	0.02	0.09	0.42	2.66	4.75	0.21	0.68	0.06	99.53
2	L13	75.40	0.05	14.10	0.93	0.06	0.07	0.32	3.76	4.08	0.16	0.82	0.07	99.82
3	M5B	73.70	0.31	13.50	2.10	0.05	0.40	0.84	2.77	4.46	0.25	1.10	0.12	99.60
4	Hzb1	73.30	0.21	14.40	1.25	0.02	0.26	0.73	3.11	5.31	0.25	0.95	0.08	99.86
5	ARN	73.10	0.18	14.60	1.43	0.04	0.33	0.65	3.12	4.86	0.33	1.07	0.11	99.82
6	IMS-1	72.95	0.31	10.41	5.25	0.11	0.05	0.22	4.73	4.46	0.02	0.49	0.11	99.11
7	Lu-1	72.70	0.18	14.50	1.23	0.02	0.34	0.69	2.82	6.14	0.17	0.97	0.12	99.88
8	L2	71.70	0.38	14.00	2.44	0.03	0.79	1.26	2.65	5.37	0.15	0.91	0.09	99.77
9	EHR-2	71.50	0.25	15.00	1.56	0.03	0.49	1.98	3.44	4.51	0.09	0.75	0.14	99.73
10	NE4	70.00	0.52	15.10	2.45	0.03	0.72	0.99	2.56	5.62	0.29	1.02	0.10	99.40
11	TI-2	69.70	0.43	15.10	2.57	0.05	0.92	2.44	3.46	3.80	0.16	0.97	0.11	99.71
12	PAG	68.60	0.51	15.20	3.02	0.05	1.06	2.51	3.25	3.99	0.19	1.15	0.15	99.67
13	428	68.16	0.58	14.88	3.86	0.06	1.39	1.77	3.31	3.98	0.19	1.29	0.20	99.67
14	SD1	67.90	0.59	15.30	3.56	0.04	1.35	1.60	2.71	4.79	0.29	1.37	0.08	99.58
15	TM2	65.60	0.51	14.61	3.49	0.06	3.41	3.11	3.54	3.74	0.17	1.28	0.14	99.66
16	PADR1	64.90	1.25	14.78	5.14	0.07	1.31	2.53	2.81	4.92	0.49	1.03	0.18	99.42
17	603	64.36	0.59	16.65	4.08	0.05	1.38	4.56	2.64	3.45	0.16	1.59	0.15	99.66
18	DP68	64.14	0.66	15.62	4.34	0.08	2.22	4.03	3.60	3.32	0.20	1.22	0.15	99.58
19	599	62.85	0.41	17.60	4.10	0.11	0.42	1.70	4.35	7.18	0.10	0.71	0.17	99.69
20	Cs-2	62.16	0.27	18.67	2.86	0.09	0.64	1.62	4.89	7.40	0.16	0.53	0.24	99.52
21	Cs-3	61.43	0.37	18.13	3.34	0.10	0.93	2.22	3.90	7.68	0.23	0.71	0.25	99.29
22	1317	60.54	0.50	17.58	4.21	0.08	2.31	3.44	3.86	4.90	0.31	1.24	0.36	99.33
23	DP49	59.04	0.90	16.85	6.32	0.10	3.55	5.72	4.10	2.26	0.25	0.95	0.11	100.15
24	1325	58.63	0.63	16.53	6.05	0.10	2.56	4.55	3.88	4.73	0.43	1.02	0.09	99.20
25	WSN1	57.67	0.99	17.31	5.43	0.08	3.17	5.07	3.77	3.48	0.42	1.80	0.20	99.39
26	594	56.83	0.89	17.65	8.43	0.18	2.59	6.16	3.32	1.49	0.25	1.44	0.43	99.66
27	Fü1b	56.60	1.48	16.20	6.82	0.11	3.74	5.84	3.28	2.91	0.51	1.74	0.16	99.39
28	GM1684	56.34	1.28	16.87	8.50	0.14	2.35	4.82	4.75	3.26	0.33	n.a.	n.a.	98.64
29	DP71	55.66	1.14	18.00	7.36	0.14	2.77	6.73	4.56	1.62	0.41	1.33	0.23	99.95
30	R4b	55.60	1.49	17.90	7.23	0.11	4.33	5.93	2.57	2.19	0.38	1.56	0.15	99.43
31	DP65	55.45	1.00	17.12	7.31	0.13	4.51	6.51	3.60	1.96	0.34	1.77	0.11	99.81
32	1327	54.51	0.82	17.13	7.40	0.13	3.59	5.99	3.49	4.34	0.54	1.22	0.11	99.27
33	TMZ1	53.57	1.05	16.74	7.03	0.11	6.53	7.16	2.69	2.02	0.39	1.69	0.16	99.13
34	598	53.17	0.41	15.95	7.94	0.15	5.53	10.55	2.25	1.54	0.11	1.81	0.31	99.72
35	KH49	53.07	0.26	15.26	10.64	0.23	0.21	2.49	8.61	4.76	0.02	2.09	0.14	97.79
36	597	49.95	0.91	17.90	9.59	0.17	4.17	8.16	3.22	3.27	0.38	1.56	0.19	99.47
37	Cs-1	48.12	0.94	8.21	7.48	0.14	10.14	14.70	1.30	3.07	2.59	1.37	0.23	98.29
38	Rhu4	48.10	0.25	16.60	4.75	0.08	12.25	15.79	0.95	0.03	0.01	0.77	0.12	99.70
39	EDB1	47.52	1.45	15.89	11.62	0.17	6.30	7.65	3.99	0.65	0.18	3.89	0.12	99.44
40	FTG1	46.75	2.88	14.84	13.09	0.20	6.04	8.69	2.51	0.93	0.45	3.01	0.11	99.49
41	GM1803	44.57	2.95	16.79	15.90	0.19	5.08	7.68	3.69	1.12	0.48	n.a.	n.a.	98.45
42	Rhu2	44.45	0.14	23.29	4.81	0.06	12.07	12.22	1.26	0.08	0.02	1.09	0.20	99.69
43	1319	43.69	1.27	17.89	11.38	0.18	6.39	11.40	2.43	1.92	0.95	1.56	0.10	99.16
44	SRH1	43.58	0.53	5.64	11.29	0.18	23.04	8.44	0.71	0.64	0.13	4.81	0.26	99.25
45	FRS1	39.20	0.25	9.70	11.96	0.16	24.14	5.82	0.52	0.05	0.03	7.29	0.32	99.44

Note. n.a. = not analyzed.

Since the method applied in this study is strictly applicable only to rocks characterized by values of λ corresponding in all directions, special care was spent to prove the isotropic nature of the samples. First, λ of every rock sample was measured at both air and water saturated in three directions that were at an angle of 90° to each other. Measurements yielded in each case values that were identical within the uncertainty of the method ($\leq$3–5%). Second, two polished thin sections were manufactured from every sample that were as well oriented 90° to each other. These sections were studied by optical microscopy, which revealed no indication for a textured appearance and any preferred orientation or alignment of rock-forming minerals or microcracks. A potential λ anisotropy triggered by flow texture was also the reason for excluding volcanic rocks from this study.

10.1029/2018JB016287

Table 3
Measured Bulk Thermal Conductivity ($\lambda_{b.meas}$), Porosity (ϕ), and Modal Mineralogy (vol.%) of Samples

#	Sample #	$\lambda_{b.meas}$ W/(mK)	φ %	Qtz %	Ab %	An %	Or %	Mc %	Anl %	Ne %	Di %	Aug %	Hbl %	Ol %	Prh %	Bt %	Ms/Ill %	Chl %	Ap %	Mag %	Ilm %	Ats/Rt %	Atg %
1	Z5b	3.20	1.33	0.45	0.24		0.06	0.18								0.04	0.03						
2	L13	3.04	1.47	0.38	0.32		0.06	0.12								0.02	0.10						
3	M5B	3.06	1.43	0.41	0.27	0.03		0.18								0.03	0.08						
4	Hzb1	3.11	1.25	0.36	0.22	0.03	0.03	0.25								0.02	0.08	0.02					
5	ARN	2.71	2.17	0.28	0.29	0.04	0.31									0.06		0.02					
6	IMS-1	2.75	1.65	0.30	0.20	0.06	0.34						0.10										
7	Lu-1	2.82	1.69	0.32	0.21	0.04	0.04	0.31								0.03	0.04	0.01					
8	L2	2.72	1.65	0.32	0.23	0.04	0.07	0.27								0.05		0.03					
9	EHR-2	2.60	1.19	0.31	0.30	0.06	0.03	0.27								0.02		0.01					
10	NE4	2.68	1.25	0.35	0.17	0.06	0.05	0.21								0.05	0.11						
11	TI-2	2.56	1.15	0.33	0.29	0.08	0.05	0.15								0.05	0.03	0.02					
12	PAG	2.70	1.07	0.33	0.32	0.08	0.14									0.10	0.03						
13	428	2.72	1.38	0.28	0.25	0.08	0.20									0.16		0.03					
14	SD1	2.52	1.27	0.36	0.32	0.10	0.15									0.06							
15	TM2	2.64	1.73	0.18	0.30	0.10	0.18					0.03	0.10		0.11								
16	PADR1	2.38	1.25	0.34	0.28	0.12	0.17									0.07					0.02		
17	603	2.49	1.28	0.20	0.24	0.10	0.19					0.03	0.03		0.03	0.16		0.02					
18	DP68	2.35	1.05	0.25	0.29	0.17	0.19						0.05			0.05							
19	599	2.05	1.62	0.04	0.40	0.04	0.42						0.06			0.04							
20	Cs-2	2.07	0.74	0.03	0.38	0.05	0.47									0.07							
21	Cs-3	2.10	0.97	0.04	0.38	0.05	0.45						0.03			0.02				0.01			
22	1317	2.21	1.91	0.12	0.40	0.10	0.26				0.02		0.10										
23	DP49	2.11	1.21	0.14	0.39	0.22	0.12						0.05			0.07			0.01				
24	1325	2.09	1.20	0.07	0.36	0.13	0.23				0.04		0.16			0.02							
25	WSN1	2.21	1.44	0.21	0.26	0.16	0.14						0.16			0.08							
26	594	2.36	0.88	0.15	0.29	0.26	0.02					0.03	0.11		0.01	0.10		0.02					
27	Fü1b	2.28	1.24	0.16	0.25	0.20	0.05						0.12			0.21							
28	GM1684	1.91	1.16	0.04	0.20	0.39	0.17				0.08		0.03			0.05		0.03		0.01	0.02		
29	DP71	1.96	1.00	0.08	0.07	0.53	0.07				0.14		0.02			0.06			0.01		0.01		
30	R4b	2.25	0.74	0.12	0.10	0.52	0.02						0.05		0.15	0.04							
31	DP65	2.11	1.09	0.11	0.04	0.47	0.07						0.19			0.10			0.02				
32	1327	2.13	0.28	0.04	0.20	0.30	0.21				0.05		0.16			0.04							
33	TMZ1	2.18	1.24	0.08	0.04	0.44	0.01						0.26		0.15	0.02							
34	598	2.26	1.44	0.00	0.30	0.17	0.09					0.08	0.23		0.03	0.07		0.02					
35	KH49	2.10	1.43		0.14	0.15	0.22			0.23		0.10	0.16										
36	597	2.13	1.45	0.00	0.05	0.44	0.13					0.05	0.19			0.13		0.01					
37	Cs-1	2.35	2.83		0.05	0.05	0.15				0.35		0.17			0.10	0.06		0.07				
38	Rhu4	2.26	1.34		0.10	0.41					0.39			0.11									
39	EDB1	2.12	1.36		0.05	0.26	0.04		0.12		0.22						0.13	0.16				0.01	
40	FTG1	2.34	1.21	0.03	0.08	0.29	0.08					0.16	0.12			0.07		0.17					
41	GM1803	2.05	1.21		0.04	0.58					0.12			0.10		0.06		0.03		0.03	0.04		
42	Rhu2	2.15	0.99		0.05	0.70								0.24				0.01					
43	1319	2.06	1.18		0.27	0.34					0.23		0.13			0.03							
44	SRH1	2.78	1.33	0.01		0.02	0.02					0.04	0.66	0.06	0.05			0.12		0.03			
45	FRS1	2.41	1.17			0.20					0.08		0.09	0.11						0.02			0.51

Note. Qtz = quartz; Ab = albite; An = anorthite; Or = orthoclase; Mc = microcline; Anl = analcime; Ne = nepheline; Di = diopside; Aug = augite; Hbl = hornblende; Ol = olivine; Prh = prehnite; Bt = biotite; Ms/Ill = muscovite/illite; Chl = chlorite; Ap = apatite; Mag = magnetite; Ilm = ilmenite; Ats/Rt = anatase/rutile; Atg = antigorite.

To minimize analytical and measurement problems potentially associated with coarse-grained or porphyritic rocks, only fine- to medium-grained, equigranular samples were considered.

To characterize the rocks geochemically, their bulk-rock major-element compositions were determined by X-ray fluorescence analysis (PANalytical AXIOS Advanced instrument) at GFZ, Potsdam, Germany, using fused glass discs (Table 2). The quantitative modal composition was determined by X-ray powder diffraction analysis both at GFZ (PANalytical Empyrean instrument, AUTOQUAN software) and at Bureau Veritas, Wingfield, Australia (PANalytical X'Pert PRO instrument, Rietveld refinement, SIROQUANT software). Weight percentages of minerals were transferred into volume percentages using well-defined values of mineral densities (cf. Schön, 2015). Only components in excess of 1 vol.% were considered, since accessory minerals negligibly contribute to λ_b (Table 3).

Plagioclase solid solutions were discriminated into their end-members albite and anorthite. On the application of electron-probe microanalysis to determine the composition of other minerals forming solid solutions, such as amphiboles and pyroxenes, was consciously renounced, to keep the analytical effort for potential users of the results of this study feasible.

Archimedes method was applied to compute density and porosity (φ) from the difference between dry, water-saturated, and submerged weights. Systematic error of porosity determination averaged to $<$0.1 vol.% absolute. Mineral thermal conductivities used in this study are compiled in Figure 1.

The optical scanning technology (thermal-conductivity scanner, TCS; Popov et al., 1999, 2016) was used for measuring rock thermal conductivity under ambient conditions (20 °C, 1 atm.). In preparation for this method, rock samples were cut to pieces of $\geq$4 cm thickness and black painted as an optical coating that unifies the optical reflection coefficients of the rock components. The λ_b data compiled in Table 4 represent the arithmetic means from 3 to 5 replicate measurements on each sample under (distilled) water-saturated conditions. Reproducibility was between 2% and 3%. For reaching water saturation, samples were first dried in a vacuum oven (60 °C, 0.01 bar, 48 hr) and then evacuated and saturated in an excicator (10 mbar at 20 °C) for a minimum of two full days. After each measurement line, the sensor was recalibrated, the scanning line was moved by 1–2 mm, to gauge a representative rock conductivity value, with-the samples being re-saturated prior to every measurement, to prevent systematic deviations according to near-surface dehydration. Additionally, a gabbro standard of 2.41 W/(mK) provided by the TCS manufacturer (Lippmann and Rauen GbR, Schaufling, Germany) was measured in parallel as controlling sample. Measurement runs for which the gabbro reference value was meet within ±2% were considered for the arithmetic-mean calculation of the samples. Absolute and relative error are reported with arithmetic mean value and 2σ standard deviation.

3. Results

We scrutinized in a first step, which mean model provides the best match between measured and calculated λ in case that porosity is not considered, that is, we compared the correspondence between $\lambda_{m.calc}$ and $\lambda_{b.meas}$. This approach was undertaken in all previous trials, which involved crystalline rocks with porosity values $<$1.5% (Chopra et al., 2018; Ray et al., 2015).

All mean models shared the common feature that they overestimate $\lambda_{m.calc}$, but at strongly varying magnitude. From all examined models, only the harmonic-mean (HM) model provided an acceptable fit, with a relative error of 5.8 ± 10.0% (2σ) and an absolute error of 6.4 ± 8.3% (2σ; Table 4 and Figure 2). Deviations range between −5.5% and 13.1%. The other models gave rise to considerably larger uncertainties, display corresponding relative and absolute errors, and are ranked as follows (error in parentheses): HSL (15 ± 13%), GM (17 ± 15%), VRH (20 ± 17%), HS (21 ± 17%), SQR (25 ± 21%), HSU (27 ± 21%), Eff (30 ± 25%), and AM (34 ± 28%).

In a second step, we verified the quantitative impact that consideration of porosity would have on the quality of fit between $\lambda_{b.calc}$ and $\lambda_{b.meas}$. Bulk thermal conductivity was computed from $\lambda_{m.calc}$ and porosity according to the equations from the three best-fitting matrix mean models (HM, HSL, and GM). Taking advantage of the results of step 1, we used $\lambda_{m.calc}$ derived from the HM model as first component and λ_f of 0.604 W/(mK) for tap water as second component. This approach resulted in a statistically

#	Sample #	$\lambda_{b.meas}$	Absolute error (%) to $\lambda_{b.meas}$					
			$\lambda_{m.calc}$			$\lambda_{b.calc}$ with HM matrix		
		W/(mK)	HM	HSL	GM	HM	HSL	GM
1	Z5b	3.20	3.4%	17.7%	22.4%	2.4%	0.6%	1.1%
2	L13	3.04	0.6%	13.5%	17.5%	5.1%	2.2%	1.8%
3	M5B	3.06	1.7%	15.6%	19.9%	4.0%	1.1%	0.7%
4	Hzb1	3.11	1.7%	10.9%	14.8%	6.4%	4.0%	3.7%
5	ARN	2.71	1.3%	13.3%	16.5%	6.0%	2.4%	2.0%
6	IMS-1	2.75	3.6%	15.5%	18.8%	2.4%	0.7%	1.0%
7	Lu-1	2.82	3.5%	16.2%	19.8%	2.8%	0.4%	0.8%
8	L2	2.72	8.4%	21.5%	25.3%	1.9%	5.3%	5.6%
9	EHR-2	2.60	9.3%	23.0%	26.7%	4.7%	7.1%	7.3%
10	NE4	2.68	10.9%	23.8%	27.7%	5.7%	8.4%	8.7%
11	TI-2	2.56	11.5%	26.9%	31.0%	6.9%	9.2%	9.5%
12	PAG	2.70	2.5%	15.7%	19.3%	1.3%	0.6%	0.8%
13	428	2.72	0.8%	11.2%	14.3%	5.4%	3.1%	2.8%
14	SD1	2.52	12.3%	27.3%	31.5%	7.3%	9.8%	10.1%
15	TM2	2.64	1.0%	9.3%	11.2%	4.7%	1.9%	1.6%
16	PADR1	2.38	10.4%	25.5%	29.2%	6.0%	8.2%	8.4%
17	603	2.49	3.7%	13.3%	15.4%	0.4%	1.6%	1.8%
18	DP68	2.35	7.4%	20.6%	23.6%	4.0%	5.7%	5.8%
19	599	2.05	11.4%	13.5%	13.8%	6.6%	8.8%	9.0%
20	Cs-2	2.07	7.1%	9.6%	10.0%	5.1%	6.1%	6.1%
21	Cs-3	2.10	10.4%	10.6%	10.7%	7.4%	8.8%	8.9%
22	1317	2.21	9.2%	15.9%	17.3%	3.3%	6.2%	6.4%
23	DP49	2.11	7.2%	14.6%	15.9%	3.7%	5.4%	5.5%
24	1325	2.09	12.1%	18.2%	19.1%	8.4%	10.2%	10.3%
25	WSN1	2.21	13.1%	25.0%	27.6%	8.2%	10.6%	10.8%
26	594	2.36	0.4%	9.0%	10.4%	2.1%	0.9%	0.8%
27	Fü1b	2.28	2.8%	10.7%	12.1%	0.7%	1.0%	1.1%
28	GM1684	1.91	12.2%	18.6%	19.0%	9.0%	10.5%	10.6%
29	DP71	1.96	8.8%	17.7%	18.4%	6.2%	7.4%	7.5%
30	R4b	2.25	2.9%	6.3%	7.3%	4.8%	3.9%	3.9%
31	DP65	2.11	1.1%	8.7%	9.5%	1.7%	0.4%	0.3%
32	1327	2.13	3.0%	8.0%	8.4%	2.2%	2.6%	2.6%
33	TMZ1	2.18	4.7%	12.9%	13.5%	1.2%	2.9%	3.0%
34	598	2.26	2.4%	6.1%	6.1%	1.6%	0.3%	0.5%
35	KH49	2.10	3.8%	6.3%	6.0%	0.1%	1.9%	1.9%
36	597	2.13	2.7%	0.0%	0.2%	6.1%	4.5%	4.5%
37	Cs-1	2.35	12.9%	20.3%	20.7%	3.0%	7.8%	8.2%
38	Rhu4	2.26	10.5%	24.2%	25.1%	6.0%	8.2%	8.4%
39	EDB1	2.12	10.0%	23.0%	23.2%	5.8%	7.8%	8.0%
40	FTG1	2.34	8.4%	19.1%	20.1%	4.3%	6.3%	6.5%
41	GM1803	2.05	4.4%	13.1%	13.3%	1.2%	2.7%	2.8%
42	Rhu2	2.15	5.5%	1.9%	1.9%	7.6%	6.6%	6.6%
43	1319	2.06	10.3%	16.7%	16.8%	6.8%	8.5%	8.6%
44	SRH1	2.78	11.7%	16.3%	17.1%	5.9%	8.9%	9.3%
45	FRS1	2.41	3.2%	8.6%	8.9%	0.5%	1.3%	1.5%

Figure 1. Absolute error from mixing-model application for calculation of matrix λ ($\lambda_{m.calc}$) from modal analysis (left) and for calculation of bulk λ ($\lambda_{b.calc}$) from HM matrix and porosity (right). Warmer colors refer to smaller deviation, colder colors to larger deviation.

significant improvement of the goodness of fit between $\lambda_{b.calc}$ and $\lambda_{b.meas}$ in case that λ_m and λ_f were calculated from the HM model (Table 4 and Figure 2). Interestingly, any of the three mean model applied to treat the fluid phase gave rise to similarly good agreement. This result also holds for all other mixing models introduced in section 2 (Braune, 2016).

Table 4
Mineral Thermal Conductivities

Phases or end-members	λ (W/[mK])	Source
Quartz	7.64	1
Albite	2.12	1
Anorthite	1.69	1
Orthoclase	2.33	1
Microcline	2.49	2
Analcime	1.27	3
Nepheline	1.50	3
Magnetite	4.92	1
Apatite	1.49	1
Dioside	4.48	1
Olivine	4.57	3
Augite	4.24	1
Hornblende	2.81	1
Prehnite	3.58	1
Biotite	2.03	1
Chlorite	5.17	1
Muscovite/illite	2.36	1
Antigorite	2.46	3
Ilmenite	2.51	1
Anatase/rutile	5.01	1

Note. 1 = mean value of Chopra et al. (2018); 2 = Brigaud & Vasseur (1989); 3 = Horai (1971).

The relative and absolute errors between $\lambda_{b.meas}$ and $\lambda_{b.calc}$ from the HM model amount to 1.4 ± 9.7% and 4.4 ± 4.9% (2σ), respectively. For all 45 samples, the deviations are <10% (−7.6 to 9.0%; Figure 2).

4. Discussion

With respect to the mixing model and the closeness of agreement, the outcome of our study is in full harmony with those of Chopra et al. (2018), who assessed 21 granites and granitic gneisses (SiO_2 > 67 wt.%) of abnormally low porosity (<0.3%) from the Bundelkhand craton in central India, and Ray et al. (2015), who surveyed 26 samples representing low-porosity (<1.5%) high-grade orthometamorphic rocks of amphibolite to granulite facies from the Indian Southern Granulite Province. The few other studies tackling this problem in crystalline rocks (Horai & Baldridge, 1972; Pribnow & Umsonst, 1993; Zhao et al., 2016) considered a smaller number of samples and came out with a poorer degree of agreement of the applied mean models, which most probably is related to the fact that the HM model was not taken into account.

Our study corroborates previous approaches not only in terms of the best-suited mean model and the magnitude of mean error (Figure 3) but also with respect to model ranking:

This study: $\lambda_{b.meas} \sim \lambda_{HM} < \lambda_{HSL} < \lambda_{GM} < \lambda_{VRH} \leq \lambda_{HS} < \lambda_{SQR} < \lambda_{HSU} < \lambda_{Eff} < \lambda_{AM}$

Chopra et al. (2018): $\lambda_{m.meas} \sim \lambda_{HM} < \lambda_{HSL} < \lambda_{GM} < \lambda_{VRH} < \lambda_{Eff} < \lambda_{HS} < \lambda_{HSU} < \lambda_{AM}$

Ray et al. (2015): $\lambda_{m.meas} \sim \lambda_{HM} < \lambda_{HSL} \leq \lambda_{GM} < \lambda_{Eff} < \lambda_{HS} < \lambda_{HSU} < \lambda_{AM}$

Notably, a comparable comprehensive study in sedimentary rocks yielded contrasting results, with the GM model providing by far the best fit between $\lambda_{b.meas}$ (water-saturated conditions) and $\lambda_{b.calc}$ (Fuchs et al., 2013).

The HM model is based on a sheet model representing a layered structure of phases, where the heat flow passes perpendicular (HM) with respect to the plane boundaries. The model is independent of the pore structure and constitute a special case (boundary) of Wiener's mixing law (Wiener, 1912), which applies to both isotropic and anisotropic mixtures. The model was introduced by Reuss (1929) to define the lower λ boundary. Considering the physical rationale of this model it was not necessarily foreseeable that the HM model provides the best fit for a medium where λ is direction independent. That this unexpected result is anyhow related to a preferred alignment of holes or cracks in the lower micrometer or nanometer scale could be excluded, since porosity accounts for only 0.1–0.2 mW/m^2 of $\lambda_{b.calc}$ depending on the applied model. Taking into account that all models overestimate $\lambda_{m.meas}$ we have examined whether use of mineral thermal conductivities lower than those listed in Table 4 (cf. Chopra et al., 2018), but within the range of values reported for a specific phase, would have an effect on model performance. For several samples, the use of lower mineral thermal conductivities would indeed result in a still better fit between $\lambda_{b.meas}$ and $\lambda_{b.calc}$, but the relative differences between the performance of the models remained virtually unchanged.

The reason for the better performance of the HM model relative to the, for instance, direction-independent GM model is still not fully understood. One possible explanation involves the assumption that the unsystematic (chaotic) arrangement of the mineral grains provokes that the heat is transported through an isotropic rock in a fashion and in a quantity as it would do perpendicular to the plane boundaries in an anisotropic medium, that is, is considerably retarded as consequence of countless heat-refraction events.

5. Conclusions and Implications

Indirect calculation of λ_b from precisely quantified modal mineralogy and porosity is demonstrated a viable option to retrieve thermal conductivity data with an acceptable amount of error. The use in thermal modeling

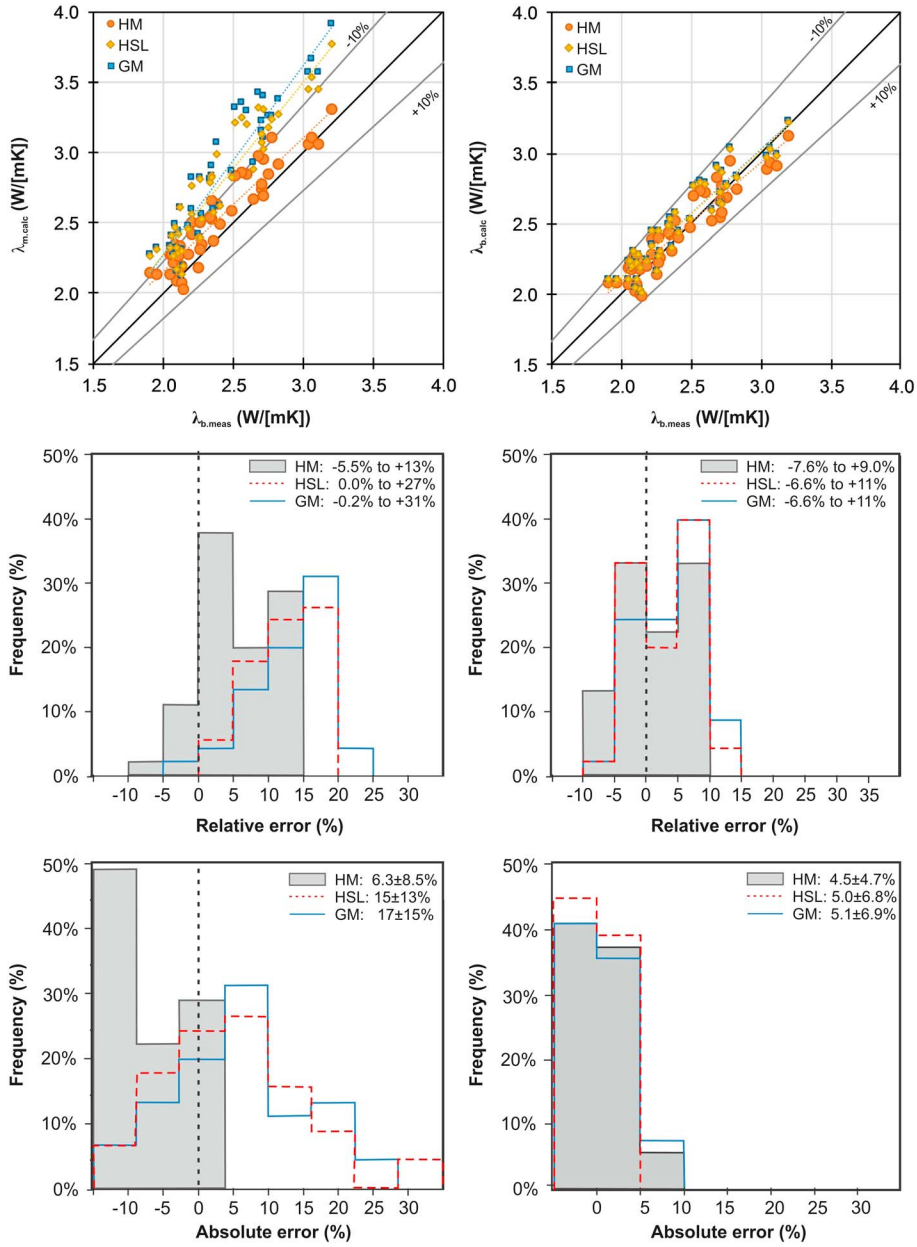

Figure 2. Comparison of the goodness of fit of those three mixing models (HM, GM, and HSL) providing the best match between $\lambda_{m.calc}$ from modal mineralogy and $\lambda_{m.calc}$ from $\lambda_{m.meas}$ (left panel) and $\lambda_{b.calc}$ (using $\lambda_{m.calc}$ from the HM model combined with $\lambda_{f.calc}$ as derived from application of the HM, HSL, and GM mixing models; right panel). Top: Cross-plots of measured versus calculated λ. Middle and bottom: Histograms of relative and absolute errors, respectively. See text for further explanations.

of such generated data, even being less accurate than laboratory measured λ values, is rated favorably relative to considering literature compilations. From the most widely examined mean models, deployment of the HM model is demonstrated giving rise to proper λ_b values for the entire suite of low-porosity crustal plutonic igneous rocks irrespective of being mafic or silicic (Figure 4). Since this model also properly works for high-grade orthometamorphic rocks (Ray et al., 2015), it is reasonable to conjecture that it yields acceptable results also for metamorphic equivalents of igneous rocks. This inference also holds for the extrusive (volcanic) equivalents of the here studied plutonic rocks as well as mantle rocks as long they are not anisotropic.

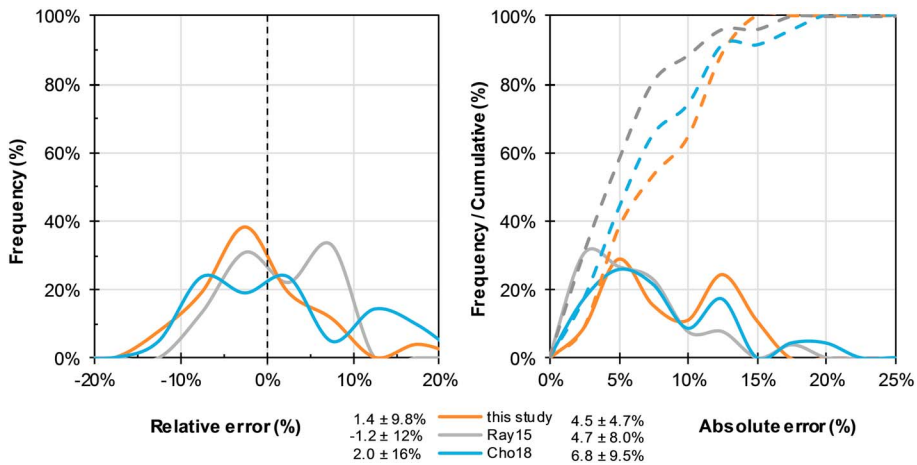

Figure 3. Comparison of relative (left) and absolute (right) errors resulting from the application of the HM model for computing λ_b for igneous rocks (this study, Chopra et al., 2018/Cho18) and metamorphic rocks (Ray et al., 2015/Ray15). Numbers denote to mean ± 2σ standard deviation.

One implication of this study is that X-ray diffraction (XRD) data on modal mineralogy, if precise and accurate, could be converted into rock thermal conductivities with uncertainties of commonly <15% (2σ) by application of the HM model, even if information on porosity is missing. In case that porosity data for modal-mineralogy samples are available or could be acquired, the amount of uncertainty is further reduced by several % to values of normally <10%. Notwithstanding, calculation of λ_b could never supersede its laboratory measurement, but it as well could not be judged an exercise not worth to conduct.

A significant implication of our study is that heat-flow data could be obtained from undisturbed and uncored boreholes, for which equilibrium T-logs and cuttings are available. Although direct measurement of λ_m is possible, this approach is time-consuming and afflicted with uncertainties on the same order as inherent in our method (Popov et al., 2018). If such drillings have exposed isotropic crystalline rocks, cuttings from all penetrated types of rock could be analyzed for quantitative modal mineralogy and eventually also porosity (for instance, from well logs or by direct measurement if size permits) and their λ inferred with the uncertainties discussed above.

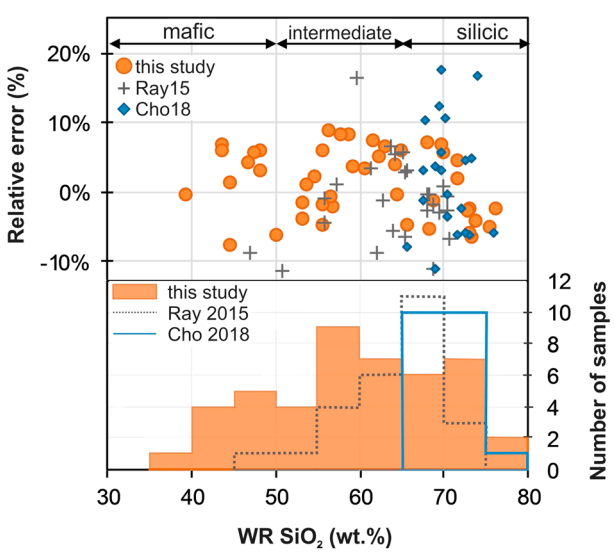

Figure 4. (top) Relative errors of $\lambda_{b.calc}$ in relation to whole-rock SiO_2 contents. See Figure 3 for abbreviations of data sources. (bottom) Histogram portraying the number of studied samples.

To exemplify the quantitative uncertainties in terms of heat flow and T associated with the approach presented in this paper, we have computed a suite of geotherms for a synthetic, 20-km-thick upper~middle continental crustal section composed of typical plutonic rocks, ranging from granite in the uppermost crust to gabbro in the basal part (Figure 5). Surface heat flow was set to 60 mW/m^2, an average value for Phanerozoic-stabilized continental crust. Adopting the HM model for both calculations of λ_m (illustrating the case of lacking porosity data) and λ_b and, considering the respective mean relative model errors reported in section 3, would result in 2σ-uncertainties in T-prediction at the middle crust-lower crust boundary of roughly ±10 °C ($\lambda_{b\text{-}calc}$) resp. ± 20 °C ($\lambda_{m.calc}$) relative to geotherms based on $\lambda_{b.meas}$ (Figures 5a and 5b). Use of the second best fitting model (HSL) would already significantly enlarge the prediction range to ~70 °C. In terms of heat flow, uncertainties would be on the order of ±7 ($\lambda_{m.calc}$) and ±5% ($\lambda_{b\text{-}calc}$), which are well within the error range accepted by the IHFC for heat-flow determination (Haenel et al., 1988; cf. Figure 5d). These percentages translate into acceptable uncertainties in heat-flow of roughly ±5 ($\lambda_{m.calc}$) and ±3 mW/m^2 ($\lambda_{b.calc}$; Figure 5c). Heat-flow calculations based on the HSL model are afflicted with uncertainties already exceeding 10% (Figure 5d).

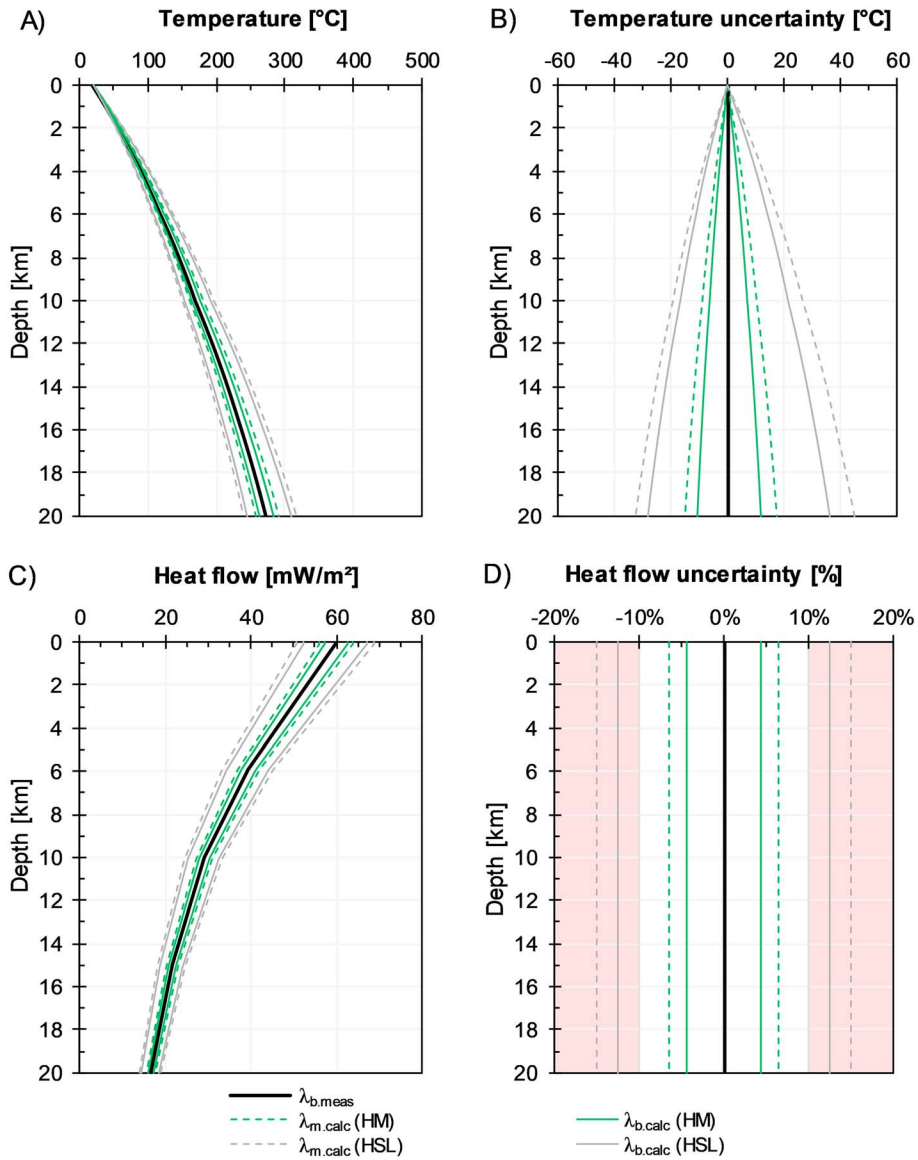

Figure 5. Uncertainties associated with the use of calculated versus measured rock thermal conductivities ($\lambda_{b.meas}$, bold black lines) on T-prediction (A + B) and heat-flow calculation (C + D) in the upper-middle continental crust. Geotherms were computed according to the well-established Chapman (1986) method and were performed for the two best-fitting models (HM and HSL) for calculation of matrix ($\lambda_{m\text{-}calc}$, stippled) and bulk thermal conductivity ($\lambda_{b\text{-}calc}$, full lines). The 20-km-thick synthetic crustal model consists, from top to bottom, of (λ in W/[mK]; heat production in μW/m^3) 6 km granite (3.0; 3.5), 4 km granodiorite (2.7; 2.5), 5 km monzodiorite (2.2; 1.5), and 5 km gabbro (2.1; 1.0). Terrestrial surface heat flow was set to 60 mW/m^2, a mean value for Phanerozoic-consolidated continental domains. (a) Geotherms computed on the basis of measured and calculated λ. (b) Temperature uncertainties associated with model uncertainties (cf. Figure 1; considered mean errors: 4.4% for HM, 12.5% for HSL); (c) heat-flow family calculated from geotherms in Figure 5A; and (d) relative uncertainty in heat-flow calculation; red-shaded areas is the error in heat-flow determination violating the criteria for validity by the IHFC (Haenel et al., 1988).

Another interesting area of application of the results of this study is the estimation of λ_b of material that was brought up to the surface from deeper parts of the crust or the upper mantle as xenoliths or enclaves. These pieces of rock are usually small in size and thermally or mechanically cracked and thus poorly suited for direct measurement. On the other hand, they are normally sufficiently big in volume that their modal mineralogy could be determined by XRD. Thus, if not re-equilibrated or otherwise

chemically altered, indirectly derived data on their thermal conductivity are essential in more properly constraining the thermal state of lithosphere domains.

Finally, Chopra et al. (2018) stated that plutonic rocks other than granites have to be studied before a substantiated statement on the overall viability of the HM model for acceptably inferring λ_b of crystalline rocks could be drawn. The results of this study provide a big step forward to such a robust conclusion.

Acknowledgments
The authors declare no financial conflicts of interests. We wish to thank W. Siebel (Freiburg) and Michael A. W. Marks (Tübingen) for providing sample material. Several staff members of Sections 6.2 (Geothermal Energy Systems) and 4.2 (Inorganic and Isotope Geochemistry) of GFZ Potsdam offered valuable support during sample preparation and XRF/XRD analysis. Associate Editor Yves Bernabe and two anonymous reviewers are thanked for constructive criticism, which supported to improve this manuscript. The data (Fuchs et al., 2018) of this study can be obtained from Research Data Repository of GFZ Data Services: http://doi.org/10.5880/GFZ.6.2.2018.005.

References

Abdulagatova, Z. Z., Abdulagatov, I. M., & Emirov, S. N. (2009). Effect of temperature and pressure on the thermal conductivity of sandstone. *International Journal of Rock Mechanics and Mining Sciences*, *46*(6), 1055–1071.

Albert, K., Franz, C., Koenigsdorff, R., & Zosseder, K. (2017). Inverse estimation of rock thermal conductivity based on numerical microscale modeling from sandstone sections. *Engineering Geology*, *231*, 1–8. https://doi.org/10.1016/j.enggeo.2017.10.010

Anand, J., Somerton, W. H., & Gomaa, E. (1973). Predicting thermal conductivities of formations from other known properties. *Journal of the Society of Petroleum Engineers*, *13*(05), 267–273. https://doi.org/10.2118/4171-PA

Braune, K. (2016). Calculation of thermal conductivity of magmatic rocks from its modal composition (Master's thesis). University of Potsdam, Institute of Earth and Environmental Sciences (in German).

Brigaud, F., & Vasseur, G. (1989). Mineralogy, porosity and fluid control on thermal conductivity of sedimentary rocks. *Geophysical Journal International*, *98*(3), 525–542. https://doi.org/10.1111/j.1365246X.1989.tb02287.x

Bruggeman, D. A. G. (1935). Berechnung verschiedener physikalischer Konstanten von heterogenen Substanzen. I. Dielektrizitätskonstanten und Leitfähigkeiten der Mischkörper aus isotropen Substanzen. *Annalen der Physik*, *416*(7), 636–664. https://doi.org/10.1002/andp.19354160705

Chapman, D. S. (1986). Thermal gradients in the continental crust. *Geological Society, London, Special Publications*, *24*(1), 63–70. https://doi.org/10.1144/gsl.sp.1986.024.01.07

Chopra, N., Ray, L., Satyanarayanan, M., & Elangovan, R. (2018). Evaluate best-mixing model for estimating thermal conductivity for granitoids from mineralogy: A case study for the granitoids of the Bundelkhand craton, central India. *Geothermics*, *75*, 1–14. https://doi.org/10.1016/j.geothermics.2018.03.011

Clauser, C. (2009). Heat transport processes in the earth's crust. *Surveys in Geophysics*, *30*(3), 163–191. https://doi.org/10.1007/s10712-009-9058-2

Drury, M. J., & Jessop, A. M. (1983). The estimation of rock thermal conductivity from mineral content—An assessment of techniques. *Zentralblatt für Geologie und Paläontologie*, *1*, 35–48.

Evans, T. R. (1977). Thermal properties of North Sea rocks. *The Log Analyst*, *18*(2), 3–12.

Fuchs, S., Balling, N., & Förster, A. (2015). Calculation of thermal conductivity, thermal diffusivity and specific heat capacity of sedimentary rocks using petrophysical well logs. *Geophysical Journal International*, *203*(3), 1977–2000. https://doi.org/10.1093/gji/ggv403

Fuchs, S., & Förster, A. (2014). Well-log based prediction of thermal conductivity of sedimentary successions: A case study from the north German Basin. *Geophysical Journal International*, *196*(1), 291–311. https://doi.org/10.1093/gji/ggt382

Fuchs, S., Förster, H.-J., Braune, K., & Förster, A. (2018). Calculation of thermal conductivity of low-porous igneous rocks from modal mineralogy. GFZ Data Services. https://doi.org/10.5880/GFZ.6.2.2018.005

Fuchs, S., Schütz, F., Förster, H.-J., & Förster, A. (2013). Evaluation of common mixing models for calculating bulk thermal conductivity of sedimentary rocks: Correction charts and new conversion equations. *Geothermics*, *47*, 40–52. https://doi.org/10.1016/j.geothermics.2013.02.002

Gegenhuber, N., & Kienler, M. (2017). Improved petrographic-coded model and its evaluation to determine a thermal conductivity log. *Acta Geophysica*, *65*(1), 103–118. https://doi.org/10.1007/s11600-017-0010-4

Goss, R., Combs, J., & Timur, A. (1975), Prediction of thermal conductivity in rocks from other physical parameters and from standard geophysical well logs. Transactions SPWLA 16th Annual Logging Symposium.

Haenel, R., Rybach, L., & Stegena, L. (1988). *Handbook of terrestrial heat-flow density determination*. Dordrecht, Netherlands: Kluwer Academic Publishers. https://doi.org/10.1007/978-94-009-2847-3

Hartmann, A., Rath, V., & Clauser, C. (2005). Thermal conductivity from core and well log data. *International Journal of Rock Mechanics and Mining Sciences*, *42*(7–8), 1042–1055. https://doi.org/10.1016/j.ijrmms.2005.05.015

Hashin, Z., & Shtrikman, S. (1962). A variational approach to the theory of the elastic behaviour of multiphase materials. *Journal of the Mechanics and Physics of Solids*, *11*(2), 127–140. https://doi.org/10.1016/0022-5096(63)90060-7

Hill, R. (1952). The elastic behaviour of a crystalline aggregate. *Proceedings of the Physical SocietySection A*, *65*, 349–354.

Horai, K.-I. (1971). Thermal conductivity of rock-forming minerals. *Journal of Geophysical Research*, *76*(5), 1278–1308. https://doi.org/10.1029/JB076i005p01278

Horai, K. I., & Baldridge, S. (1972). Thermal conductivity of nineteen igneous rocks, II estimation of thermal conductivity of rock from the mineral and chemical compositions. *Physics of the Earth and Planetary Interiors*, *5*, 157–166. https://doi.org/10.1016/0031-9201(72)90085-4

Lichtenecker, K. (1924). Der elektrische Leitungswiderstand künstlicher und natürlicher Aggregate.*Physikalische Zeitschrift*, *25*, 169–181, 193–204, 226–233.

Popov, E., Trofimov, A., Goncharov, A., Abaimov, S., Chekhonin, E., Popov, Y., & Sevostianov, I. (2018). Technique of rock thermal conductivity evaluation on core cuttings and non-consolidated rocks. *International Journal of Rock Mechanics and Mining Sciences*, *108*, 15–22. https://doi.org/10.1016/j.ijrmms.2018.05.005

Popov, Y., Beardsmore, G., Clauser, C., & Roy, S. (2016). ISRM suggested methods for determining thermal properties of rocks from laboratory tests at atmospheric pressure. *Rock Mechanics and Rock Engineering*, *49*(10), 4179–4207. https://doi.org/10.1007/s00603-016-1070-5

Popov, Y. A., Pribnow, D. F. C., Sass, J. H., Williams, C. F., & Burkhardt, H. (1999). Characterization of rock thermal conductivity by high-resolution optical scanning. *Geothermics*, *28*(2), 253–276. https://doi.org/10.1016/S0375-6505(99)00007-3

Pribnow, D., & Umsonst, T. (1993). Estimation of thermal conductivity from the mineral composition: Influence of fabric and anisotropy. *Geophysical Research Letters*, *20*, 2199–2202. https://doi.org/10.1029/93GL02135

Pribnow, D., Williams, C. F., & Burkhardt, H. (1993). Well log-derived estimates of thermal conductivity in crystalline rocks penetrated by the 4-km deep KTB Vorbohrung. *Geophysical Research Letters*, *20*, 1155–1158. https://doi.org/10.1029/93GL00480

Ray, L., Förster, H.-J., Förster, A., Fuchs, S., Naumann, R., & Appelt, O. (2015). Tracking the thermal properties of the lower continental crust: Measured versus calculated thermal conductivity of high-grade metamorphic rocks (southern Granulite Province, India). *Geothermics*, *55*, 138–149.

Reuss, A. (1929). Berechnung der Fließgrenze von Mischkristallen auf Grund der Plastizitätsbedingung für Einkristalle. *Zeitschrift für Angewandte Mathematik und Mechanik*, *9*(1), 49–58. https://doi.org/10.1002/zamm.19290090104

Roy, R. F., Beck, A. E., & Touloukain, Y. S. (1981). Thermophysical properties of rocks. In Y. S. Touloukain, W. R. Judd, & R. F. Roy (Eds.), *Physical properties of rocks and minerals* (pp. 409–502). New York: McGraw-Hill Cindus.

Schön, J. H. (2015). *Physical properties of rocks: A workbook*. Amsterdam, Netherlands: Elsevier.

Voigt, W. (1928). *Lehrbuch der Kristallphysik*. Leipzig: Teubner.

Wiener, O. H. (1912). Die Theorie des Mischkörpers für das Feld der stationären Strömung. *Abhandlungen der Mathematisch-Physischen Klasse der Königlich-Sächsischen Gesellschaft der Wissenschaften* (Vol. 32(6), 604 pp.). Leipzig: Teubner.

Williams, C. F., & Anderson, R. N. (1990). Thermophysical properties of the Earth's crust: In situ measurements from continental and ocean drilling. *Journal of Geophysical Research*, *95*, 9209–9236. https://doi.org/10.1029/JB095iB06p09209

Zhao, X. G., Wang, J., Chen, F., Li, P. F., Ma, L. K., Xie, J. I., & Liu, Y. M. (2016). Experimental investigations on the thermal conductivity characteristics of Beishan granitic rocks for China's HLW disposal. *Tectonophysics*, *683*, 124–137. https://doi.org/10.1016/j.tecto.2016.06.021